Energy Advances

PAPER

View Article Online
View Journal | View Issue

Cite this: *Energy Adv.*, 2024, 3, 2035

Slow hole diffusion limits the efficiency of p-type dye-sensitized solar cells based on the P1 dye†

Maria B. Brands,[a] Olivier C. M. Lugier,[a] Kaijian Zhu,[b] Annemarie Huijser,[b] Stefania Tanase[a] and Joost N. H. Reek*[a]

Received 30th April 2024,
Accepted 1st July 2024

DOI: 10.1039/d4ya00271g

rsc.li/energy-advances

NiO electrodes are widely applied in p-type dye-sensitized solar cells (DSSCs) and photoelectrochemical cells, but due to excessive charge recombination, the efficiencies of these devices are still too low for commercial applications. To understand which factors induce charge recombination, we studied electrodes with a varying number of NiO layers in benchmark P1 p-DSSCs. We obtained the most efficient DSSCs with four layers of NiO (0.134%), and further insights into this optimum were obtained *via* dye loading studies and *in operando* photoelectrochemical immittance spectroscopy. These results revealed that more NiO layers led to an increasing light harvesting efficiency (η_{LH}), but a decreasing hole collection efficiency (η_{CC}), giving rise to the maximum efficiency at four NiO layers. The decreasing η_{CC} with more NiO layers is caused by longer hole collection times, which ultimately limits the overall efficiency. Notably, the recombination rates were independent of the number of NiO layers, and similar to those observed in the more efficient n-type DSSC analogues, but hole collection was an order of magnitude slower. Therefore, with more NiO layers, the beneficial increase in η_{LH} can no longer counteract the decrease in η_{CC} due to slow hole collection, resulting in the overall efficiency of the solar cells to maximize at four NiO layers.

Introduction

NiO is commonly used as a p-type semiconducting photocathode in solar-energy harvesting devices, such as dye-sensitized solar cells (DSSCs) and dye-sensitized photoelectrochemical cells.[1–3] The efficiencies of p-type and tandem DSSCs (4.1%[4]) are still limited, especially compared to that of n-type DSSCs, which recently reached over 15%.[5] Excessive charge recombination at the photocathode is the main reason for the poor performance of tandem and p-type devices. To prevent this recombination, efforts have been put into rationally designing the molecular components of these devices. For instance, the push–pull character of a photosensitizer supports spatial separation of electrons and holes, thereby reducing charge recombination to some extent.[6–8] Photosensitizers equipped with binding motifs to pre-organize the electrolyte *via* pseudo-rotaxane formation also result in spatial separation of charges, similarly reducing charge recombination and thus improving the overall efficiency.[9] Furthermore, alternative p-type semiconductor materials have been investigated, including $CuCrO_2$[10,11] or indium-doped tin oxide (ITO).[12,13] Although these materials are very promising in terms of transparency and hole mobility, they are still outperformed by NiO, which possesses a combination of characteristics that are crucial for an efficient photocathode, such as a good transparency and surface area, and high stability in various solvent systems.[7]

Several groups have thus focused on the optimization of NiO photocathodes, where efforts have been put into designing the optimal preparation route for the NiO electrode, which can greatly impact the DSSC efficiency.[14–16] To facilitate comparison between different NiO electrodes in p-type DSSCs, a benchmark system has been developed, in which NiO has been sensitized with the P1 dye.[14,17] The working principle of the overall p-DSSC based on P1 is schematically shown in Fig. 1(a), where the photocathode is typically combined with a Pt counter anode[18,19] and an iodide/triiodide redox couple in a sandwich

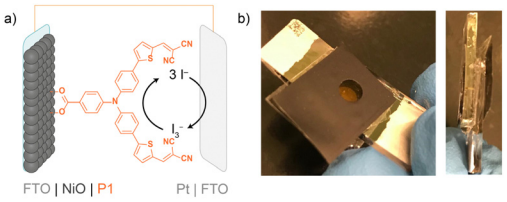

Fig. 1 (a) Schematic overview of the P1 p-DSSC benchmark system; (b) the sandwich DSSC, left: top view; right: side view.

[a] *Van't Hoff Institute for Molecular Sciences, University of Amsterdam, Science Park 904, 1098 XH Amsterdam, The Netherlands. E-mail: j.n.h.reek@uva.nl*
[b] *MESA+ Institute for Nanotechnology, University of Twente, Hallenweg 23, 7522 NH, Enschede, The Netherlands*

† Electronic supplementary information (ESI) available. See DOI: https://doi.org/10.1039/d4ya00271g

cell, as depicted in Fig. 1(b). Although these solar cells do not lead to record efficiencies, this benchmark system is valuable in understanding the influence of the NiO preparation route on the performance of the photocathode. Previous benchmark studies concluded that doctor-blading of a $NiCl_2$ sol–gel precursor solution leads to the most efficient P1-based p-DSSCs.[14,15]

In general, during doctor-blading, a $NiCl_2$ precursor solution is applied on a conduction substrate (FTO) using a tape mask, after which the resulting sol–gel is sintered, and this process is repeated as often as desired. However, the exact experimental details of the optimal preparation still seem to be under debate. For instance, several reports suggest that two layers of the nickel sol–gel solution should be applied,[20–26] whereas others apply one,[27] three,[28–30] or 'multiple'[31–34] layers. Furthermore, even when the reported preparation method is exactly the same, the efficiencies of the resulting solar cells tend to vary significantly.[14,20,35] It is also known that the quality of NiO can vary significantly when prepared by different researchers while using the same procedure.[6,36]

We therefore revisit the preparation of NiO electrodes *via* doctor-blading. In this context, we optimized the method by studying how the number of NiO layers influences the performance of the photocathode in the benchmark P1 p-DSSC. To obtain deeper insights into the efficiency-limiting factors, the charge transfer dynamics were investigated with photoelectrochemical impedance spectroscopy (PEIS), and intensity-modulated photocurrent and photovoltage spectroscopy (IMPS and IMVS). These *in operando* methods have been combined often for n-type DSSCs, to obtain a better understanding of the charge dynamics on the solar cell efficiency.[37–51] On the other hand, the hole kinetics of the benchmark P1 p-DSSC has exclusively been characterized *in operando* with PEIS,[52] whereas IMPS and IMVS can be valuable complementary methods. We thus investigated the kinetics of the photogenerated holes by combining these three methods, from which we obtained important insights on how the charge dynamics influence the performance of the solar cell. To the best of our knowledge, this is the first study that addresses the influence of the NiO doctor-blading method on the *in operando* charge dynamics and overall efficiency of p-DSSCs.

Results and discussion

P1-sensitized NiO electrodes with one to five layers of NiO were synthesized and characterized, and their performance was subsequently evaluated in the benchmark P1 p-DSSCs. We tested their performance by measuring the *J–V* curves of the solar cells, and we also determined the thickness and dye loading of the electrodes. Finally, the charge dynamics were investigated with IMPS and PEIS.

Somewhat unconventional, we classified the NiO electrodes according to the number of doctor-blade cycles instead of their thickness, where the latter is more common in the literature. Although the film thickness is a very relevant property, it can be an impractical point of reference, since there appears to be no general consensus on the optimal value.[20,25–34] More importantly, we found that a reproduced film thickness does not automatically result in a similarly performing electrode (*vide infra*). On the other hand, classifying the electrodes by the number of NiO layers lies close to practice, and is a more straightforward target to aim for than for a certain film thickness. Furthermore, this categorization still directly relates to the film thickness, but includes additional relevant parameters,[20] such as the film porosity and density.

Synthesis, characterization and assembly of the P1-sensitized p-DSSCs

Since the exact preparation route is very relevant for reproduction of the results below, we have provided a detailed experimental description on our electrode preparation procedure in the ESI.† The first step of the NiO electrode preparation is the electrodeposition of a thin layer (<100 nm) of NiO on fluorine doped tin oxide (FTO).[53] The surface roughness of this thin NiO layer enhances the connection between the porous NiO film and the FTO substrate, allowing for efficient charge transfer, essential for the performance of the DSSC. Subsequently, the mesoporous NiO film was applied *via* doctor-blading according to the method of Sun *et al.*,[20] but instead of two layers, one to five layers were applied (in quadruple). Each set was named after the number of doctor-bladed NiO layers; the samples consisting of one layer of NiO is referred to as the NiO1 set. The electrodes were characterized with scanning electron microscopy (Fig. SI-4 and SI-5, ESI†). The thickness was determined with a profilometer (see the ESI,† Section 2.1). As expected, the average NiO film thickness increases with the number of layers (Table 1). The P1 dye was then grafted on the NiO surface by dipping the electrode in a P1 dye solution in acetonitrile for 16 hours.[20] Visual inspection of the electrodes showed that these turned from light grey into bright red (see Table SI-1, ESI†).

The P1 dye loading generally increases with the NiO layers, as was determined by dye leaching studies under mild conditions (Table 1).[54–56] The P1 dye loadings on the electrodes reported herein are well within the range of earlier reported values (see Table SI-4, ESI†).[57–61] Remarkably, comparison of NiO5 and NiO4 shows that the dye loading did not increase, while the NiO5 film is thicker. A possible explanation can be found by closely inspecting the SEM images in Fig. SI-5 (ESI†). When carrying out multiple rounds of doctor blading, the bottom NiO layers are exposed to high temperatures repeatedly. The particles in these bottom layers will continue to sinter and grow. After four layers, larger pores seem to form in the bottom

Table 1 Average thickness and P1 dye loading of the electrodes with varying numbers of doctor-bladed NiO layers

Sample group	Film thickness (μm)	P1 loading (nmol cm^{-2})
NiO1	0.63 ± 0.06	75.31 ± 20.11
NiO2	0.93 ± 0.23	74.91 ± 12.31
NiO3	1.30 ± 0.34	111.28 ± 34.19
NiO4	1.58 ± 0.32	143.37 ± 25.74
NiO5	2.16 ± 0.14	130.39 ± 15.74

layers, which will negatively influence the available surface area and thus dye loading. The inferior dye loading observed for sample NiO5 compared to NiO4 is thus likely the result of this reduced available surface area, which is not compensated for by the increase in the film thickness. These results also illustrate the relevance of the number of doctor blade cycles on the porosity and film density, and why we thus prefer to assort the NiO electrodes accordingly.

Efficiency of benchmark p-DSSCs

The P1-sensitized electrodes were assembled in sandwich cells (Fig. 1(b)) and their performance was assessed by measuring the *J–V* curve while illuminated with 100 mW cm^{-2} white LED light (emission spectrum in Fig. SI-11, ESI†). The open-circuit potential (V_{OC}), short-circuit current density (J_{SC}), fill factor (FF), and power conversion efficiency (η) were extracted from the *J–V* data (eqn (SI-2) and (SI-3), ESI†). We also investigated the performance of solar cells with a similar NiO thickness (within 0.05 μm difference), to see if a reproduced film thickness leads to a reproduced photocathode performance, but the results were rather divergent (Tables SI-12, ESI†). The results categorized on the number of NiO layers are shown in Table 2. The values have been averaged for the various sample groups, with the values of the most efficient solar cell of the corresponding set in parentheses. Details of the individual solar cells can be found in the ESI.†

Notably, the average solar cell efficiencies (η) vary significantly, showing an upward trend from 0.087% observed for NiO1 up to the maximum of 0.134% (NiO4), followed by a slight drop to 0.121% for NiO5. To find out which factors dictate this efficiency, we examined the correlation between η and V_{OC}, FF and J_{SC} (see Fig. SI-13, ESI†). V_{OC} varies considerably between the different sample groups (101–119 mV), but no clear correlation with η could be found. Similarly, the fill factor varies between 0.277–0.318, but also did not show a clear link to η. On the other hand, we observed a linear dependency of η on J_{SC} (Fig. SI-13, ESI†). On average, an increase in photocurrent was observed from −2.19 mA cm^{-2} for NiO1, to −4.49 mA cm^{-2} for NiO4, followed by a slight decrease for NiO5 to −4.15 mA cm^{-2}, which is a similar trend to that observed for η. Clearly, the solar cell efficiency strongly depends on the short-circuit photocurrent, and therefore we decided to investigate the fundamental elements of the photocurrent in more detail.

The measured photocurrent is a result of multiple light-harvesting and charge separation processes in the p-DSSC, as described by eqn (1):[62,63]

$$J = q \cdot \eta_{inj} \cdot \phi_{reg} \cdot \eta_{CC} \int I_0(\lambda) \cdot \eta_{LH}(\lambda) d\lambda \quad (1)$$

where q is the elementary charge, η_{inj} is the hole injection efficiency from the excited dye into NiO, ϕ_{reg} is the dye regeneration yield, η_{CC} is the charge collection efficiency, I_0 is the photon flux, and η_{LH} is the light harvesting efficiency. Since the same dye, semiconductor, redox mediator and light source are used in all solar cells, we assume that q, η_{inj}, ϕ_{reg} and I_0 are similar or identical in all cases.[63] However, η_{LH} and η_{CC} strongly depend on the dye loading and film thickness, respectively, which vary significantly for the different NiO sets (Table 1).

η_{LH} is related to the dye loading according to eqn (2):[64]

$$\eta_{LH}(\lambda) = 1 - 10^{-\Gamma\sigma(\lambda)} \quad (2)$$

where Γ represents the dye loading (in moles per cm^2 of illuminated surface area) of the film, and $\sigma(\lambda)$ is the absorption cross-section in units of cm^2 mol^{-1}, obtained from the decadic extinction coefficient (ε in M^{-1} cm^{-1}) by multiplication with 10^3 cm^3 L^{-1}. The η_{LH} spectra (Fig. SI-9, ESI†) show that most light is harvested by the NiO4 electrodes, as determined by integration of the η_{LH} (λ) response (see Table SI-5, ESI†). Interestingly, due to the very high ε of P1 between 330 and 530 nm, this part of the η_{LH} (λ) spectrum reaches a light harvesting efficiency of 1 when the dye loading is >111.28 nmol cm^{-2}. At wavelengths longer than 530 nm, the light harvesting efficiency is the highest for NiO4, resulting in the maximum overall η_{LH} (λ).

Probing the charge collection efficiency with photoelectrochemical immittance spectroscopy

After light harvesting (*i.e.*, photoexcitation of the dye and hole injection into NiO), the hole needs to travel through the nanoporous NiO network to the conducting FTO substrate. The success of this process is described as the charge collection efficiency (η_{CC}). The average time it takes for a photogenerated hole to travel to the FTO electrode is given by the hole collection time (τ_c), as is schematically shown by the green path in Fig. 2. Ideally, this time is short, because fast hole transport can manifest on the macroscale as a high photocurrent. Alternatively, the photogenerated hole can recombine with electrons from species in the electrolyte or at the surface of the NiO

Table 2 Averaged performance of the P1 p-DSSCs with a varying number of NiO layers, as derived from the *J–V* curves. The values for the individual solar cells can be found in the ESI, as well as how the values were extracted from the *J–V* data. The values in parentheses represent the data of the solar cell with the highest performance in that data set

Sample group	η (%)	J_{SC} (mA cm^{-2})	V_{OC} (mV)	FF
NiO1	0.075 ± 0.029 (0.096)	−2.19 ± 0.82 (−2.948)	106 ± 9 (107)	0.318 ± 0.010 (0.307)
NiO2	0.093 ± 0.020 (0.114)	−2.59 ± 0.95 (−3.196)	119 ± 20 (117)	0.316 ± 0.037 (0.303)
NiO3	0.087 ± 0.046 (0.133)	−2.94 ± 1.36 (−4.254)	101 ± 7 (106)	0.288 ± 0.028 (0.295)
NiO4	0.134 ± 0.049 (0.190)	−4.49 ± 1.45 (−6.154)	107 ± 1 (107)	0.277 ± 0.017 (0.289)
NiO5	0.121 ± 0.031 (0.143)	−4.15 ± 0.81 (−4.724)	105 ± 2 (106)	0.278 ± 0.013 (0.295)

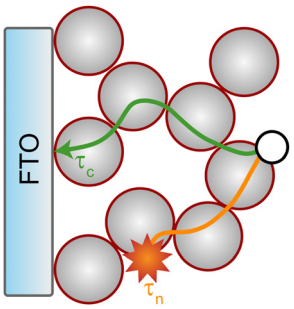

Fig. 2 Schematic overview of the hole collection pathway (green) and the hole recombination pathway (orange) in the dye-sensitized photocathode. The dye-sensitized NiO nanoparticles are represented by the red circles filled with grey, and the photogenerated hole is shown as the empty circle. The competition between these two processes is described by the charge collection efficiency (η_{CC}).

particle. The electron–hole pair generated by light absorption is then lost at the expense of the solar cell efficiency. The average time it takes for a photogenerated hole to recombine with an electron is given by the hole lifetime (τ_n).[65] A long τ_n with respect to τ_c is beneficial, since it means that most of the holes will be collected before recombination occurs. This competition between the charge collection and recombination is expressed by the charge collection efficiency (eqn (3)).[66,67]

$$\eta_{CC} = 1 - \frac{\tau_c}{\tau_n} \quad (3)$$

The time constants τ_c and τ_n in DSSCs can be measured *in operando* with (combinations of) the three complementary photoelectrochemical immittance techniques: intensity modulated photocurrent and photovoltage spectroscopy (IMPS and IMVS, respectively) and photoelectrochemical impedance spectroscopy (PEIS).[50,68] To understand how η_{CC} changes in DSSCs based on different NiO layers, we have determined both τ_c and τ_n (Fig. 3) under short circuit conditions (at 0 V, where the photocurrent is at its maximum).[69] The values for τ_c were determined using IMPS analysis,[70] and those for τ_n by PEIS (see Sections 3.2 and 3.3 in the ESI† for detailed procedures). Subsequently, the average η_{CC} for the different sets of solar cells was calculated, and the results are plotted in the left panel of Fig. 3.

For NiO1, a reasonable η_{CC} of 0.91 was observed, but η_{CC} decreases linearly with the number of layers, and ends up at a value of 0.65 for NiO5. The samples with the highest photocurrent (NiO4) show an average η_{CC} of 0.70. The underlying reason for this decline in η_{CC} with more NiO layers is given by the trends in τ_c and τ_n, which are plotted in Fig. 3 (right). The hole collection times τ_c are depicted in navy and the hole recombination times τ_n in orange. Interestingly, τ_n was only marginally affected by the number of NiO layers: for NiO1 the average time was 101.3 ± 13.7 ms, and for NiO5 this value decreased to 87.7 ± 6.8 ms. For NiO4, the hole recombination time was approximately 93.5 ± 33.7 ms. On the other hand, a clear trend in τ_c was observed as the number of NiO layers increased. In the NiO1 devices, it took the average hole 9.0 ± 3.0 ms to travel from the surface of the NiO particles to the FTO. For devices with thicker NiO films, this average τ_c increases: for NiO4, τ_c is as large as 28.2 ± 0.0 ms, and for NiO5 the collection time has increased to 30.3 ± 14.6 ms. The τ_c thus increases as more NiO layers are applied, but τ_n remains relatively constant. The overall result is a decline in the charge collection efficiency with more NiO layers.

These time constants and charge collection efficiencies are in line with earlier reports on the charge dynamics of similar p-DSSCs.[28,31,32,52,67,71–75] However, the results stand in strong contrast with the η_{CC} observed for n-type DSSCs, which is typically close to 1, even when relatively thick films (8 μm) of semiconductor material are used.[76] This excellent charge

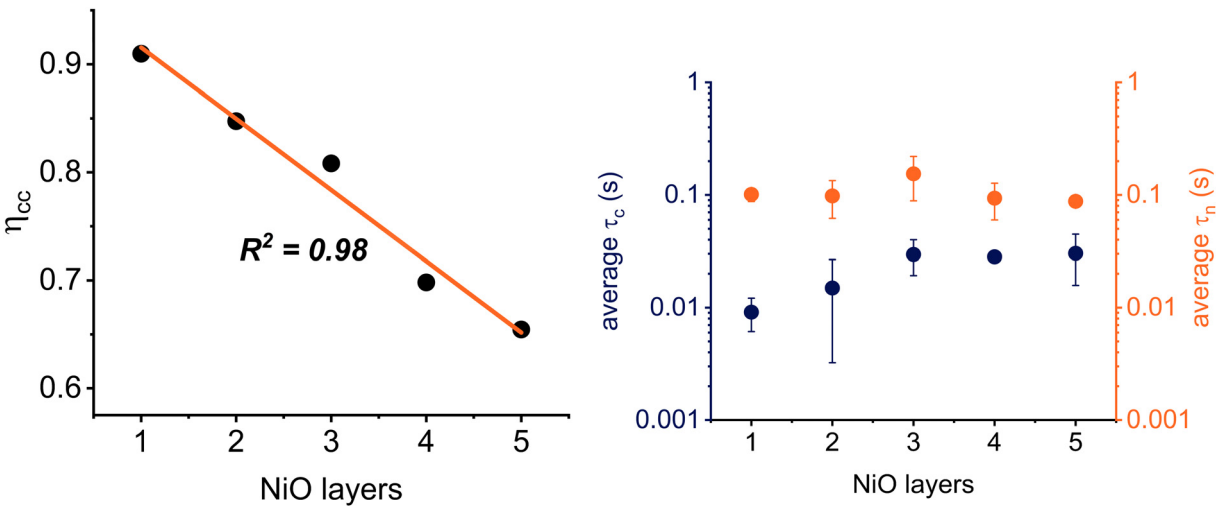

Fig. 3 Left: The charge collection efficiency η_{CC} *versus* the number of NiO layers; right: variation of the hole collection time τ_c (navy) and hole recombination time τ_n (orange) as a function of the number of applied NiO layers.

collection efficiency in n-type DSSCs arises from a favourable τ_n/τ_c ratio, which frequently lies above 10^2. Interestingly, we found that τ_n in our p-DSSCs is close to those in n-type solar cells (0.1 *vs.* 0.2 s, respectively). τ_c, however, is an order of magnitude faster in the n-type DSSCs (10^{-3} s). In n-type DSSCs, the photogenerated charges are thus collected up to thirtyfold faster, even though the film thickness is at least fourfold higher. The recombination times are thus comparable to those in n-type DSSCs, whereas the τ_c values are remarkably slow. This slow τ_c causes more holes to recombine, limits η_{CC}, and causes the photocurrent to be more than a factor two lower, at -4.49 mA cm^{-2} for NiO4, compared to typical n-type DSSCs.[76]

The limiting factors of the p-DSSC efficiency

In summary, the solar cell efficiency, which strongly depends on the short-circuit current, showed an optimum at NiO4. With an increase in the number of NiO layers, the dye loading rises, resulting in an increased light harvesting efficiency (η_{LH}). The dye loading was the highest for NiO4, which could explain the high photocurrents observed for this sample group. Besides the dye loading, other factors regarding the homogeneity of the film might influence the performance of the electrode, such as the changing porosity of the bottom layers during multiple doctor blading and sintering cycles. For instance, Fig. SI-5 (ESI†) shows that the cracks in the NiO films of NiO1 and NiO2 disappear after three or more doctor-blading cycles. Furthermore, upon examination of the connection between the NiO film and the FTO surface, gaps could be observed for NiO1, NiO2 and NiO3. After four doctor-blade cycles or more, these gaps were absent. The good homogeneity of the NiO4 films, combined with appropriate connection to the FTO surface, could thus also positively influence the electrode performance.

Meanwhile, the charge collection efficiency (η_{CC}) steadily dropped as the NiO film thickness increased, due to the longer hole diffusion length. The relatively long hole diffusion time of NiO caused more holes to recombine as the hole diffusion length increased. Therefore, the low η_{CC}, caused by slow hole collection and an unfavourable hole diffusion–recombination ratio, currently limits the photocurrent of the NiO photocathode in this benchmark P1-sensitized p-DSSC.

Furthermore, the efficiency of our DSSCs is also limited by the low V_{OC}, which is determined by the difference in energy between the NiO valence band and the I^-/I_3^- redox potential. With the NiO electrode preparation optimized, further improvement in the efficiency should be achieved by (1) shortening the hole collection time by increasing the hole diffusion rate constant, (2) using dyes that absorb a broader part of the solar spectrum, (3) increasing the V_{OC} by adjusting the potential of the redox mediator,[77] and (4) implementing strategies that lead to active charge separation in these devices, as also described in the introduction.[6–9]

Conclusions and outlook

To find out how NiO photocathodes are limiting the efficiency of dye-sensitized solar cells (DSSCs), we have thoroughly characterized the properties of the benchmark P1 p-DSSCs, while varying the number of doctor-bladed NiO layers. Analysis of the *J–V* curves showed that the most efficient solar cells were obtained with four layers of NiO (NiO4) on FTO. The DSSC efficiency showed a linear relation with the short-circuit current density; the higher the J_{SC}, the higher the efficiency. Partially in line with the trend observed for the J_{SC}, the light harvesting efficiency (η_{LH}) increased with the NiO film thickness, and reached a maximum at NiO4. The trend in J_{SC} could be further explained by the charge collection efficiency (η_{CC}), which decreased as more layers of NiO were applied in the device. Thicker NiO films resulted in impeded hole diffusion, while the hole recombination time remained unaffected. Therefore, the optimum in solar cell efficiency at NiO4 is the result of an increasing η_{LH} as more NiO layers are applied, but a decreasing η_{CC}, which limits the average solar cell efficiency of this benchmark system to a maximum of $0.134 \pm 0.049\%$.

Future efforts could focus on improving the η_{CC} by increasing the hole lifetime or by decreasing the hole collection time. Several strategies have been reported to lower charge recombination,[9,28,32,78] including rational design of the dye and redox mediator to impose electronic repulsion between the reduced electrolyte and the dye. Furthermore, the hole transfer time could be decreased by the incorporation of conductive materials,[79,80] such as Ni–NiO core–shell structures. This latter concept is currently under investigation in our groups.

Author contributions

J. R. and M. B. conceived the project and designed the experiments. K. Z. carried out scanning electron microscopy imaging, supervised by A. H. O. L. determined the film thickness of the NiO films, supervised by S. T. M. B. prepared the electrodes, solar cells, analysed the data and wrote the manuscript, under supervision of J. R. All authors discussed the results and commented on the manuscript.

Data availability

The data supporting this article have been included as part of the ESI.†

Conflicts of interest

There are no conflicts to declare.

Acknowledgements

This work is part of the Advanced Research Center for Chemical Building Blocks, ARC CBBC, which is co-founded and co-financed by the Dutch Research Council (NWO) and the Netherlands Ministry of Economic Affairs and Climate Policy. Jaap Beerens is acknowledged for practical assistance on the profilometer measurements. We thank Dr Sonja Pullen, Dr Tessel

Bouwens, Dr Tijmen Bakker and Tom Keijer, MSc. for fruitful discussions regarding this study.

Notes and references

1 A. Belén Muñoz-García, I. Benesperi, G. Boschloo, J. J. Concepcion, J. H. Delcamp, E. A. Gibson, G. J. Meyer, M. Pavone, H. Pettersson, A. Hagfeldt and M. Freitag, *Chem. Soc. Rev.*, 2021, **50**, 12450.
2 V. Nikolaou, A. Charisiadis, G. Charalambidis, A. G. Coutsolelos and F. Odobel, *J. Mater. Chem. A*, 2017, **5**, 21077.
3 J. He, H. Lindström, A. Hagfeldt and S. E. Lindquist, *J. Phys. Chem. B*, 1999, **103**, 8940.
4 Y. Farré, M. Raissi, A. Fihey, Y. Pellegrin, E. Blart, D. Jacquemin and F. Odobel, *ChemSusChem*, 2017, **10**, 2618.
5 Y. Ren, D. Zhang, J. Suo, Y. Cao, F. T. Eickemeyer, N. Vlachopoulos, S. M. Zakeeruddin, A. Hagfeldt and M. Grätzel, *Nature*, 2023, **613**, 60.
6 E. Benazzi, J. Mallows, G. H. Summers, F. A. Black and E. A. Gibson, *J. Mater. Chem. C*, 2019, **7**, 10409.
7 K. E. Dalle, J. Warnan, J. J. Leung, B. Reuillard, I. S. Karmel and E. Reisner, *Chem. Rev.*, 2019, **119**, 2752.
8 A. Moinel, M. Brochnow, C. Aumaître, E. Giannoudis, J. Fize, C. Saint-Pierre, J. Pécaut, P. Maldivi, V. Artero, R. Demadrille and M. Chavarot-Kerlidou, *Sustainable Energy Fuels*, 2022, **6**, 3565.
9 T. Bouwens, T. M. A. Bakker, K. Zhu, J. Hasenack, M. Dieperink, A. M. Brouwer, A. Huijser, S. Mathew and J. N. H. Reek, *Nat. Chem.*, 2023, **15**, 213.
10 S. Wrede and H. Tian, *Phys. Chem. Chem. Phys.*, 2020, **22**, 13850.
11 D. Xiong, Z. Xu, X. Zeng, W. Zhang, W. Chen, X. Xu, M. Wang and Y. B. Cheng, *J. Mater. Chem.*, 2012, **22**, 24760.
12 Z. Yu, I. R. Perera, T. Daeneke, S. Makuta, Y. Tachibana, J. J. Jasieniak, A. Mishra, P. Bäuerle, L. Spiccia and U. Bach, *NPG Asia Mater.*, 2016, **8**, e305.
13 Z. Huang, M. He, M. Yu, K. Click, D. Beauchamp and Y. Wu, *Angew. Chem., Int. Ed.*, 2015, **54**, 6857.
14 C. J. Wood, G. H. Summers, C. A. Clark, N. Kaeffer, M. Braeutigam, L. R. Carbone, L. D'Amario, K. Fan, Y. Farré, S. Narbey, F. Oswald, L. A. Stevens, C. D. J. Parmenter, M. W. Fay, A. La Torre, C. E. Snape, B. Dietzek, D. Dini, L. Hammarström, Y. Pellegrin, F. Odobel, L. Sun, V. Artero and E. A. Gibson, *Phys. Chem. Chem. Phys.*, 2016, **18**, 10727.
15 D. Dini, Y. Halpin, J. G. Vos and E. A. Gibson, *Coord. Chem. Rev.*, 2015, **304–305**, 179.
16 M. Bonomo, G. Naponiello, I. Venditti, V. Zardetto, A. Di Carlo and D. Dini, *J. Electrochem. Soc.*, 2017, **164**, H137.
17 K. S. Keremane, Y. Pellegrin, A. Planchat, D. Jacquemin, F. Odobel and A. Vasudeva Adhikari, *J. Phys. Chem. C*, 2022, **126**, 12383.
18 C. Y. Lin, J. Y. Lin, C. C. Wan and T. C. Wei, *Electrochim. Acta*, 2011, **56**, 1941.
19 D. F. Bruggeman, T. M. A. Bakker, S. Mathew and J. N. H. Reek, *Chem. – Eur. J.*, 2021, **27**, 218.
20 L. Li, E. A. Gibson, P. Qin, G. Boschloo, M. Gorlov, A. Hagfeldt and L. Sun, *Adv. Mater.*, 2010, **22**, 1759.
21 F. Wu, L. Zhu, S. Zhao, Q. Song and C. Yang, *Dyes Pigm.*, 2016, **124**, 93.
22 Y. Hao, C. J. Wood, C. A. Clark, J. A. Calladine, R. Horvath, M. W. D. Hanson-Heine, X.-Z. Sun, I. P. Clark, M. Towrie, M. W. George, X. Yang, L. Sun and E. A. Gibson, *Dalton Trans.*, 2016, **45**, 7708.
23 L. Zhu, H. B. Yang, C. Zhong and C. M. Li, *Dyes Pigm.*, 2014, **105**, 97.
24 F. A. Black, C. A. Clark, G. H. Summers, I. P. Clark, M. Towrie, T. Penfold, M. W. George and E. A. Gibson, *Phys. Chem. Chem. Phys.*, 2017, **19**, 7877.
25 P. Qin, J. Wiberg, E. A. Gibson, M. Linder, L. Li, T. Brinck, A. Hagfeldt, B. Albinsson and L. Sun, *J. Phys. Chem. C*, 2010, **114**, 4738.
26 L. Tian, T. Törndahl, J. Lin, P. B. Pati, Z. Zhang, T. Kubart, Y. Hao, J. Sun, G. Boschloo and H. Tian, *J. Phys. Chem. C*, 2019, **123**, 26151.
27 L. D'Amario, G. Boschloo, A. Hagfeldt and L. Hammarström, *J. Phys. Chem. C*, 2014, **118**, 19556.
28 Q. Liu, L. Wei, S. Yuan, X. Ren, Y. Zhao, Z. Wang, M. Zhang, L. Shi and D. Li, *J. Mater. Sci.*, 2015, **50**, 6668.
29 L. Wei, L. Jiang, S. Yuan, X. Ren, Y. Zhao, Z. Wang, M. Zhang, L. Shi and D. Li, *Electrochim. Acta*, 2016, **188**, 309.
30 M. Zannotti, E. Benazzi, L. A. Stevens, M. Minicucci, L. Bruce, C. E. Snape, E. A. Gibson and R. Giovannetti, *ACS Appl. Energy Mater.*, 2019, **2**, 7345.
31 Z. Huang, G. Natu, Z. Ji, M. He, M. Yu and Y. Wu, *J. Phys. Chem. C*, 2012, **116**, 26239.
32 E. A. Gibson, A. L. Smeigh, L. Le Pleux, L. Hammarström, F. Odobel, G. Boschloo and A. Hagfeldt, *J. Phys. Chem. C*, 2011, **115**, 9772.
33 E. A. Gibson, L. Le Pleux, J. Fortage, Y. Pellegrin, E. Blart, F. Odobel, A. Hagfeldt and G. Boschloo, *Langmuir*, 2012, **28**, 6485.
34 K. A. Click, D. R. Beauchamp, B. R. Garrett, Z. Huang, C. M. Hadad and Y. Wu, *Phys. Chem. Chem. Phys.*, 2014, **16**, 26103.
35 S. Sumikura, S. Mori, S. Shimizu, H. Usami and E. Suzuki, *J. Photochem. Photobiol., A*, 2008, **199**, 1.
36 R. Brisse, R. Faddoul, T. Bourgeteau, D. Tondelier, J. Leroy, S. Campidelli, T. Berthelot, B. Geffroy and B. Jousselme, *ACS Appl. Mater. Interfaces*, 2017, **9**, 2369.
37 A. J. Frank, N. Kopidakis and J. van de Lagemaat, *Coord. Chem. Rev.*, 2004, **248**, 1165.
38 X. Y. Yu, J. Y. Liao, K. Q. Qiu, D. B. Kuang and C. Y. Su, *ACS Nano*, 2011, **5**, 9494.
39 M. Raïssi, Y. Pellegrin, F. X. Lefevre, M. Boujtita, D. Rousseau, T. Berthelot and F. Odobel, *Sol. Energy*, 2020, **199**, 92.
40 R. Kern, R. Sastrawan, J. Ferber, R. Stangl and J. Luther, *Electrochim. Acta*, 2002, **47**, 4213.
41 Q. Wang, J.-E. Moser and M. Grätzel, *J. Phys. Chem. B*, 2005, **109**, 14945.
42 C. Richter, M. Beu and D. Schlettwein, *Phys. Chem. Chem. Phys.*, 2015, **17**, 1883.

43 X. Miao, K. Pan, Y. Liao, W. Zhou, Q. Pan, G. Tian and G. Wang, *J. Mater. Chem. A*, 2013, **1**, 9853.
44 G. Schlichthörl, N. G. Park and A. J. Frank, *J. Phys. Chem. B*, 1999, **103**, 782.
45 L. M. Peter and K. G. U. Wijayantha, *Electrochim. Acta*, 2000, **45**, 4543.
46 L. M. Peter, *Chem. Rev.*, 1990, **90**, 753.
47 L. Dloczik, O. Ileperuma, I. Lauermann, L. M. Peter, E. A. Ponomarev, G. Redmond, N. J. Shaw and I. Uhlendorf, *J. Phys. Chem. B*, 1997, **101**, 10281.
48 G. Franco, J. Gehring, L. M. Peter, E. A. Ponomarev and I. Uhlendorf, *J. Phys. Chem. B*, 1999, **103**, 692.
49 J. van de Lagemaat and A. J. Frank, *J. Phys. Chem. B*, 2000, **104**, 4292.
50 J. Halme, *Phys. Chem. Chem. Phys.*, 2011, **13**, 12435.
51 T. Oekermann, D. Zhang, T. Yoshida and H. Minoura, *J. Phys. Chem. B*, 2004, **108**, 2227.
52 Z. Huang, G. Natu, Z. Ji, P. Hasin and Y. Wu, *J. Phys. Chem. C*, 2011, **115**, 25109.
53 M. Bonomo, D. Di Girolamo, M. Piccinni, D. P. Dowling and D. Dini, *Nanomaterials*, 2020, **10**, 1.
54 S. Lyu, J. Massin, M. Pavone, A. B. Muñoz-García, C. Labrugère, T. Toupance, M. Chavarot-Kerlidou, V. Artero and C. Olivier, *ACS Appl. Energy Mater.*, 2019, **2**, 4971.
55 D. Ameline, S. Diring, Y. Farre, Y. Pellegrin, G. Naponiello, E. Blart, B. Charrier, D. Dini, D. Jacquemin and F. Odobel, *RSC Adv.*, 2015, **5**, 85530.
56 P. Qin, H. Zhu, T. Edvinsson, G. Boschloo, A. Hagfeldt and L. Sun, *J. Am. Chem. Soc.*, 2008, **130**, 8570.
57 L. Zhu, H. Yang, C. Zhong and C. M. Li, *Chem. – Asian J.*, 2012, **7**, 2791.
58 M. Bonomo, D. Di Girolamo, M. Piccinni, D. P. Dowling and D. Dini, *Nanomaterials*, 2020, **10**, 1.
59 J. Cui, J. Lu, X. Xu, K. Cao, Z. Wang, G. Alemu, H. Yuang, Y. Shen, J. Xu, Y. Cheng and M. Wang, *J. Phys. Chem. C*, 2014, **118**, 16433.
60 M. Bonomo, D. Gatti, C. Barolo and D. Dini, *Coatings*, 2018, **8**, 232.
61 C.-H. Chang, Y.-C. Chen, C.-Y. Hsu, H.-H. Chou and J. T. Lin, *Org. Lett.*, 2012, **14**, 4726.
62 T. Daeneke, Z. Yu, G. P. Lee, D. Fu, N. W. Duffy, S. Makuta, Y. Tachibana, L. Spiccia, A. Mishra, P. Bäuerle and U. Bach, *Adv. Energy Mater.*, 2015, **5**, 1401387.
63 K. Zhu, N. R. Neale, A. Miedaner and A. J. Frank, *Nano Lett.*, 2007, **7**, 69.
64 M. K. Nazeeruddin, A. Kay, I. Rodicio, R. Humphry-Baker, E. Müller, P. Liska, N. Vlachopoulos and M. Grätzel, *J. Am. Chem. Soc.*, 1993, **115**, 6382.
65 J. Bisquert and F. Fabregat-santiago, *J. Phys. Chem. C*, 2009, **113**, 17278.
66 R. Wang, Y. Kuwahara, K. Mori, C. Louis, Y. Bu and H. Yamashita, *J. Mater. Chem. A*, 2020, **8**, 21613.
67 Z. Hongjun, A. Hagfeldt and G. Boschloo, *J. Phys. Chem. C*, 2007, **111**, 17455.
68 D. Klotz, D. S. Ellis, H. Dotan and A. Rothschild, *Phys. Chem. Chem. Phys.*, 2016, **18**, 23438.
69 X. L. Zhang, Z. Zhang, F. Huang, P. Bäuerle, U. Bach and Y.-B. Cheng, *J. Mater. Chem.*, 2012, **22**, 7005.
70 P. A. DeSario, J. J. Pietron, D. H. Taffa, R. Compton, S. Schünemann, R. Marschall, T. H. Brintlinger, R. M. Stroud, M. Wark, J. C. Owrutsky and D. R. Rolison, *J. Phys. Chem. C*, 2015, **119**, 17529.
71 L. D'Amario, R. Jiang, U. B. Cappel, E. A. Gibson, G. Boschloo, H. Rensmo, L. Sun, L. Hammarström and H. Tian, *ACS Appl. Mater. Interfaces*, 2017, **9**, 33470.
72 G. Natu, P. Hasin, Z. Huang, Z. Ji, M. He and Y. Wu, *ACS Appl. Mater. Interfaces*, 2012, **4**, 5922.
73 Z. Liu, D. Xiong, X. Xu, Q. Arooj, H. Wang, L. Yin, W. Li, H. Wu, Z. Zhao, W. Chen, M. Wang, F. Wang, Y.-B. Cheng and H. He, *ACS Appl. Mater. Interfaces*, 2014, **6**, 3448.
74 I. Hod, Z. Tachan, M. Shalom and A. Zaban, *Phys. Chem. Chem. Phys.*, 2013, **15**, 6339.
75 L. Le Pleux, A. L. Smeigh, E. Gibson, Y. Pellegrin, E. Blart, G. Boschloo, A. Hagfeldt, L. Hammarström and F. Odobel, *Energy Environ. Sci.*, 2011, **4**, 2075.
76 J. van de Lagemaat, N. G. Park and A. J. Frank, *J. Phys. Chem. B*, 2000, **104**, 2044.
77 D. Zhang, M. Stojanovic, Y. Ren, Y. Cao, F. T. Eickemeyer, E. Socie, N. Vlachopoulos, J.-E. Moser, S. M. Zakeeruddin, A. Hagfeldt and M. Grätzel, *Nat. Commun.*, 2021, **12**, 1777.
78 L. Favereau, Y. Pellegrin, L. Hirsch, A. Renaud, A. Planchat, E. Blart, G. Louarn, L. Cario, S. Jobic, M. Boujtita and F. Odobel, *Adv. Energy Mater.*, 2017, **7**, 1601776.
79 M. Zhu, X. Li, W. Liu and Y. Cui, *J. Power Sources*, 2014, **262**, 349.
80 S. Hyung Kang, N. R. Neale, K. Zhu, A. F. Halverson, Y. Yan and A. J. Frank, *RSC Adv.*, 2013, **3**, 13342.